1-2021

Evaluating the Impacts of Dam Construction and Longshore Transport upon Modern Sedimentation within the Rio Grande Delta (Texas, U.S.A.)

Samantha Moore
The University of Texas Rio Grande Valley

Elizabeth A. Heise
The University of Texas Rio Grande Valley

Marty Grove
Stanford University

Anthony Reisinger
Texas A&M University

Jude A. Benavides
The University of Texas Rio Grande Valley

Recommended Citation

Moore, Samantha, Elizabeth A. Heise, Marty Grove, Anthony Reisinger, and Jude A. Benavides. 2020. "Evaluating the Impacts of Dam Construction and Longshore Transport upon Modern Sedimentation within the Rio Grande Delta (Texas, U.S.A.)." Journal of Coastal Research 37 (1): 26–40. https://doi.org/10.2112/JCOASTRES-D-20-00049.1.

Journal of Coastal Research	37	1	26–40	Coconut Creek, Florida	January 2021

Evaluating the Impacts of Dam Construction and Longshore Transport upon Modern Sedimentation within the Rio Grande Delta (Texas, U.S.A.)

www.cerf-jcr.org

Samantha Moore[†], Elizabeth A. Heise[†]*, Marty Grove[‡], Anthony Reisinger[§], and Jude A. Benavides[†]

[†]School of Earth, Environmental & Marine Sciences
University of Texas, Rio Grande Valley
Brownsville, TX 78412, U.S.A.

[‡]Department of Geological Sciences
Stanford University
Stanford, CA 94305, U.S.A.

[§]Harte Research Institute
Texas A&M University
Corpus Christi, TX 78412, U.S.A.

www.JCRonline.org

ABSTRACT

Moore, S.; Heise, E.A.; Grove, M.; Reisinger, A., and Benavides, J.A., 2021. Evaluating the impacts of dam construction and longshore transport upon modern sedimentation within the Rio Grande Delta (Texas, U.S.A.). *Journal of Coastal Research,* 37(1), 26–40. Coconut Creek (Florida), ISSN 0749-0208.

The modern Rio Grande delta system has experienced a century of dam construction, water removal for irrigation and municipal use, and land use modifications that have dramatically reduced its sediment load. This study examines whether damming has sufficiently limited delivery of upstream sediment to permit locally eroded sources and/or littoral transport along the coast to influence the provenance signal of the Rio Grande delta. Changes in sediment provenance within the Rio Grande's delta can be detected and quantified by measurement of detrital zircon Uranium–lead dating age distributions. Previous provenance studies indicate that modern Rio Grande river sand upstream of Falcon Dam is enriched in zircon derived from Oligocene volcanic fields within the southern Rocky Mountains and the Sierra Madre Occidental. Results from this study indicate that the abundance of Oligocene zircon is depleted in the modern Rio Grande delta relative to river sand sampled upstream of Falcon Dam. Mixing calculations performed with age distributions representative of Eocene–Miocene fluvial sedimentary deposits that crop out downstream of the dam indicate that erosional reworking of these materials has significantly altered sedimentary provenance within the delta. The importance of north-directed longshore transport along the Mexican (Tamaulipas-Veracruz) Gulf Coast was also evaluated. The absence of distinctive zircon from the Trans Mexican volcanic belt and the basement of southern Mexico within the barrier islands of the Rio Grande delta support previous conclusions that sediment transport along the Tamaulipas-Veracruz shelf is highly compartmentalized and restricted in lateral movement due to seasonal variation in littoral current polarity, topographic barriers along the shelf, and other phenomena. Nevertheless, the results of this study demonstrate that construction of dams across rivers such as the Rio Grande is capable of sufficiently limiting upstream sediment transport to permit otherwise unimportant local sources to dominate sand provenance within their delta systems.

ADDITIONAL INDEX WORDS: *Sediment starvation, longshore current, detrital zircon, U-Pb age.*

INTRODUCTION

Dam construction and the sprawl of human civilization have adversely affected the supply of river sediments to deltas in ways that are difficult to predict (e.g., Nienhuis *et al*., 2020). The Rio Grande delta is a prime example. Situated along the coast of southernmost Texas, U.S.A. and northern Tamaulipas, Mexico, the wave-dominated Rio Grande delta marks the terminus of the 3000 km long Rio Grande system (Figure 1). The modern Rio Grande delta formed primarily between 8000 and 3000 YBP as a result of a large sediment flux carried by the Rio Grande during the Holocene Climatic Optimum (Rodriguez, Fassell, and Anderson, 2001). Prior to *ca*. 1850, the Rio Grande River flowed naturally into the delta region as an alluvial channel filled with pebbly sand (Jepsen *et al*., 2003). As human population has increased, the need for flood control and stable water storage for agriculture and human habitation resulted in dam construction and a myriad of irrigation projects. These modifications of the Rio Grande system have reduced its flow and sediment flux to such an extent that it currently delivers negligible sediment to the coast (Anderson *et al*., 2014; Benke and Cushing, 2005; Jepsen *et al*., 2003).

The reduction in Rio Grande sediment flux described above coupled with the Late Holocene highstand in sea level prompts interesting questions. For example, do present-day conditions result in the Rio Grande delta receiving a significant fraction of its sediment from unexpected, and/or previously unimportant sources? This paper investigate two possibilities: (1) locally-derived sediment eroded downstream of Falcon and Marte R. Gómez dams; and (2) longshore transport of extraregional sediment transported northward along the Tamaulipas-Veracruz Gulf Coast to the Rio Grande Delta's barrier islands (Figure 1). Provenance analysis based upon the measurement of detrital zircon Uranium–lead dating (U-Pb) age distributions provides the means to detect and quantify the contributions of distinct sediment sources. In this study, detrital zircon U-Pb age distributions were measured in modern Rio Grande delta sediment and compared to previous relevant data (Blum *et al*., 2017; Fan, Brown, and Li, 2019; Mackey, Horton, and Milliken,

DOI: 10.2112/JCOASTRES-D-20-00049.1 received 16 April 2020; accepted in revision 15 August 2020; corrected proofs received 28 October 2020; published pre-print online 9 December 2020.
*Corresponding author: elizabeth.heise@utrgv.edu

Figure 1. Location map for modern Rio Grande river catchment (light blue). Mississippi River catchment is included for reference (light green). Approximate region of offshore delta sedimentation for these two rivers shown in gray (after Davis, 2017). Solid brown line represents drainage divide for rivers flowing into the Gulf of Mexico. Abbreviations for other rivers mentioned in text shown in blue font with full names provided in lower left-hand corner of figure. Western Gulf Coast segments discussed in text include Texas, Tamaupipas, and Veracruz. Black dashed line shows limit of continental shelf (130 meters) in western Gulf of Mexico. Colored dashed lines indicate approximate location of ancient shorelines of Texas along Gulf of Mexico shown for the Paleocene (green), Eocene (red), Oligocene (brown), and Miocene (purple) (adapted from Mackey, Horton, and Milliken, 2012). The Rio Grande River forms the boundary between the U.S.A. and Mexico. Outcrop area of the Trans Mexican Volcanic Belt (TVMB) is indicated in orange. Cities of Laredo (L) and Brownsville (B) are located with red squares while Falcon (F) and Marte E. Gomez (G) dams are located with bold line segments. Abbreviations of other locations mentioned in text include: Coastal Plain (CP), Colorado Plateau (CP), Cabo Rojo (CR), Great Plains (GP), Rocky Mountains (RM), Rio Grande Rift (RR), Sierra Nevada Madre Occidental (SMOc), and Sierra Madre Oriental (SMOr). Area of Figure 2 is outlined.

2012; Repasch *et al*., 2017; Xu, Stockli, and Snedden, 2017) to evaluate these hypotheses.

Cenozoic Shoreline Strata of the Texas Margin

The Texas Gulf shoreline propagated southwards throughout the Cenozoic (Galloway, Whiteaker, and Ganey-Curry, 2011) (Figure 1). Paleocene, Eocene, Oligocene, and Miocene conglomerate, sandstone, and shale deposited during this southward migration crop out in the south Texas–northern Tamaulipas region (Page, VanSistine, and Turner, 2005) (Figure 2). Provenance studies indicate that the rivers that formed these deposits drained significant regions of the continental interior throughout the Cenozoic (Blum *et al*., 2017; Fan, Brown, and Li, 2019; Mackey, Horton, and Milliken, 2012; Repasch *et al*., 2017; Xu, Stockli, and Snedden, 2017). The Early Cenozoic deposits are exposed due to deformation related to the NW-SE trending, Laramide-related, Coahuila fold belt (Ewing, 1997; Gray and Lawton, 2011; Page, VanSistine, and Turner, 2005). A series of normal-slip growth faults down drop the Eocene and the overlying Oligocene and Miocene strata to the east (Ewing, 1986; Page, VanSistine, and Turner, 2005).

Late Quaternary–Holocene Sea Level Change

The last low stand of sea level occurred between *ca*. 27–19 Ka and correlated with the maximum expansion of global ice sheets (Clark *et al*., 2009). Subsequent warming resulted in

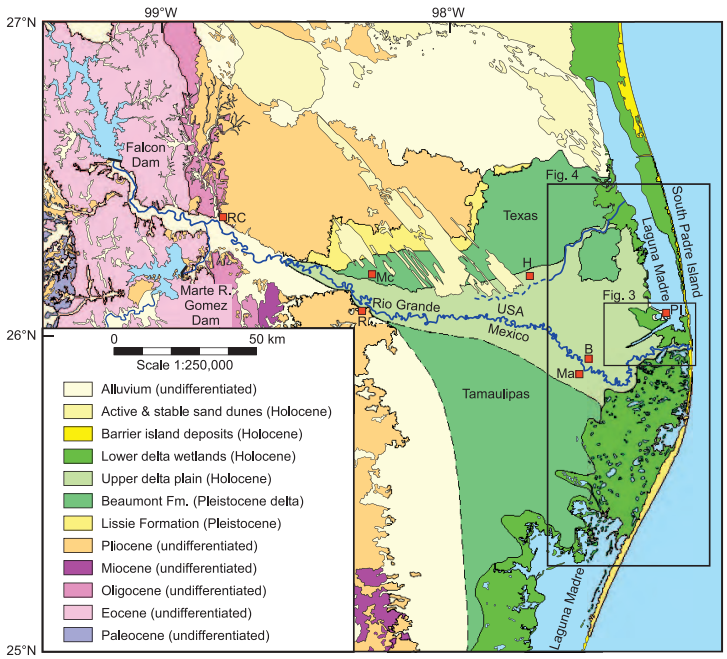

Figure 2. Geologic map of the Rio Grande Delta region. State of Texas (U.S.A.) occurs north of the Rio Grande while state of Tamaulipas (Mexico) lies south. Bedrock geology simplified from Page, VanSistine, and Turner (2005). Holocene delta geology interpreted from data in Page, VanSistine, and Turner (2005) and Ewing and Gonzalez (2016). The geometry of older Pleistocene delta deposits included within the Beaumont Formation are more approximately located, particularly on the Mexican side of the Rio Grande where there is considerable agricultural development. Falcon Dam along Rio Grande and Marte E. Gomez on Rio San Jose are shown. Locations of samples in Table 1 are shown. Locations mentioned in the text are abbreviated as follows: Brownsville (B), Harlingen (H), Port Isabel (PI), Matamoros (Ma), McAllen (Mc), Reynosa (R), and Rio Grande City (RC). Area of Figure 4 is outlined.

dramatic coastal flooding within the northern Gulf of Mexico over the past 10 ka. Age-depth relationships of estuary, marsh, and swash-zone depositional environments for the northern Gulf of Mexico indicate that sea level increased dramatically at 9 to 5 mm/year between 10–8 Ka (Milliken, Anderson, and Rodriguez, 2008). Sea level rise decreased to 5 to 2 mm/year between 8–5 Ka and has slowed to less than 0.6 mm/year over the past 5 Ka. Comparison of regional and global sea-level curves for the last 5000 years indicate that Late Holocene relative sea-level rise across the northern Gulf of Mexico cannot be explained by coastal subsidence (Milliken, Anderson, and Rodriguez, 2008). Satellite altimetry and tide-gauge records indicates that rates of sea level rise have increased by an order of magnitude over the past century (Milliken, Anderson, and Rodriguez, 2008).

Rio Grande Drainage System

The 2830 km long Rio Grande is the fifth longest river in North America (Figure 1). It has a combined catchment of 472,000 km^2 and defines a 1254 km segment of the U.S.-Mexico border. Also referred to as the Rio Bravo in Mexico, the modern Rio Grande has two hydrologic domains. The upper Rio Grande of Colorado and New Mexico is fed by snow-melt from the southern Rockies and is almost entirely depleted as it flows into west Texas. The lower Rio Grande domain begins with the confluence of the Rio Conchos (Figure 1). The Rio Conchos has a 68,386 km^2 catchment that includes the Sierra Madre Occidental in the Mexican state of Chihuahua. The water carried by the Rio Conchos is supplied by the North American Monsoon and accounts for *ca*. 50% of the water carried by the lower Rio Grande. Further downstream, the Rio Grande receives input from the Pecos River, Rio Salado, and smaller streams (Figure 1). Its last major tributary, the Rio San Juan, has a catchment of 33,538 km^2 that includes the Sierra Madre Oriental in the Mexican state of Nuevo León (Figure 1).

Rio Grande Delta

The Late Quaternary and Holocene sea level changes described above created earlier lobes of the Rio Grande delta (Banfield and Anderson, 2004; Hiatt, 2010; Rodriguez, Fassell, and Anderson, 2001; Weight, Anderson, and Fernandez, 2011). These offshore deltas are believed to have been the dominant source of sands that nourished the central Texas barriers in the past (Anderson *et al*., 2014) and may also have contributed to the south Texas coast. Alternatively, more recently deposited offshore sediment cored from the south Texas inner shelf and shoreface is composed mostly of a thin veneer of sand resting on red delta silt and clay (Rodriguez, Fassell, and Anderson, 2001). This implies that offshore sand sources are no longer major sources of coastal sediment.

The modern Rio Grande delta straddles the international U.S.-Mexico border and has an areal extent of 360,000 km^2 (Ewing and Gonzalez, 2016) (Figure 2). The Holocene delta apex is situated *ca*. 50 km west of the Gulf Coast (98° E) near Reynosa, Mexico (Figure 2). A radiating array of precursor main channels of the Rio Grande abandoned by avulsion extend eastward.

These successively developed channels have produced a 110 km swath of Holocene delta plain deposits along the N-S trending Gulf Coast (Ewing and Gonzalez, 2016) (Figure 2). The latter are built upon clay, silt, sand, and gravel of the Pleistocene Beaumont Formation that represent stream-channel, point-bar, natural-levee, and backswamp deposits of a previously developed delta (Page, VanSistine, and Turner, 2005) (Figure 2).

The Rio Grande delta can be divided into two topographic domains: the upper and lower delta plain. In the upper plain, meandering abandoned river channels, locally known as *resacas*, are bound by sand-rich levees that rise 3–5 m higher than the surrounding interchannel regions. Although the topographically lower delta plain is morphologically similar, the interchannel regions are inundated by large ephemeral shallow brackish to saline lakes referred to as *esteros* (Ewing and Gonzalez, 2016) (Figure 2).

Shoreline Environment

A nearly continuous shoreline and dune system marks the interface between the delta and the Gulf of Mexico. North of the U.S.-Mexico border, South Padre Island extends for hundreds of km along the Texas coastline. This barrier island forms lagoons that notably include Laguna Madre (Figure 2). Under fair-weather conditions, 30 to 60 cm high waves with a 2 to 6 second period strike the shoreline. The shallowly inclined, fine sand beaches generate spilling waves. The coast is affected by a diurnal, microtidal (<1 m) range (Morton, 1994).

The long axes of sand dune fields in south Texas define a bearing of 318° for the prevailing winds (Figure 2). According to the Texas Weather Atlas (Larkin and Bomar, 1983), 1961–1980 weather records from Brownville wind conditions are highly seasonal. During the winter (December–February), winds alternate from blowing out of the N to NW as weather fronts approach to S to SE during intervening periods. Wind speeds vary between 8 to 15 knots. For the spring and summer months (March to August), the prevailing winds blow out of the SE to SSE at wind speeds generally between 10–20 knots. Hurricane season lasts from June through November and peaks during August and September. During the fall, winds again alternate from N to NW to S to SE but tend to be light (6–12 knots).

The coastal winds interact with the curved shape of the Texas coastline to cause longshore currents to flow north in south Texas and west in east Texas. This results in a convergence zone offshore of central Texas (Anderson *et al*., 2014; Curray, 1960; Lohse, 1955; Rodriguez, Fassell, and Anderson, 2001). Consequently, shoreface deposits from east and south Texas are thinner and retrograding compared to those from central Texas, which are thicker and prograding (Rodriguez, Fassell, and Anderson, 2001). Hurricanes that impact southern Texas periodically increase erosion rates by up to an order of magnitude (*e.g*., Heise *et al*., 2009).

Human Impacts upon the Rio Grande Delta System

Burgeoning ranching and agriculture activity within the Rio Grande Valley prompted the establishment of the International Boundary and Water Commission in 1889. Marte R. Gómez Reservoir was constructed across the Rio San Juan, the last major tributary of the Rio Grande in 1936. Subsequent construction of Falcon Dam along the Rio Grande occurred in 1953 (Benke and Cushing, 2005) (Figure 1). Additional irrigation projects have substantially reduced the flow of the Rio Grande to the point where the mouth of the Rio Grande River has been sealed by sand bars and silted over (Benke and Cushing, 2005; Ewing and Gonzalez, 2016; Jepsen *et al*., 2003).

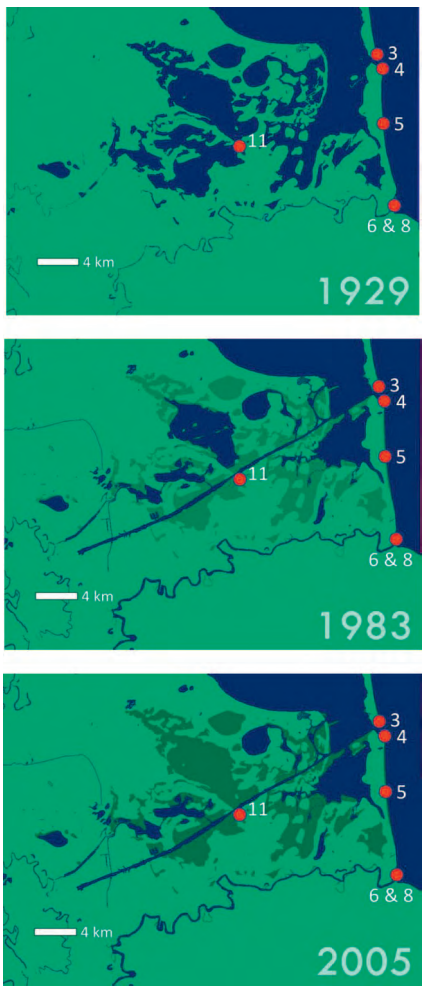

Figure 3. Morphological change of the Rio Grande delta system related to anthropogenic activity. Locations of samples #3–#8 and #11 shown: (A) Delta wetland region in 1929 prior to most dam construction; (B) 1983 conditions after creation of the Brownsville ship channel and construction of jetties and dredging of Brazos Santiago Pass; (C) 2005 conditions after continued dredging and draining of delta wetlands.

The configuration of the Rio Grande delta was considerably different in the early 1900s than it is today. Figure 3 depicts the coastline morphology in 1930s prior to most dam construction and flood control projects when the coastal interface and barrier islands were less well developed. Dewatering and dredging have significantly impacted the delta system over time (Morton and Pieper, 1975) (Figure 3). In order to ensure the viability of Brazos Santiago Pass as a navigable waterway, jetties were constructed by the Army Corps of Engineers in the

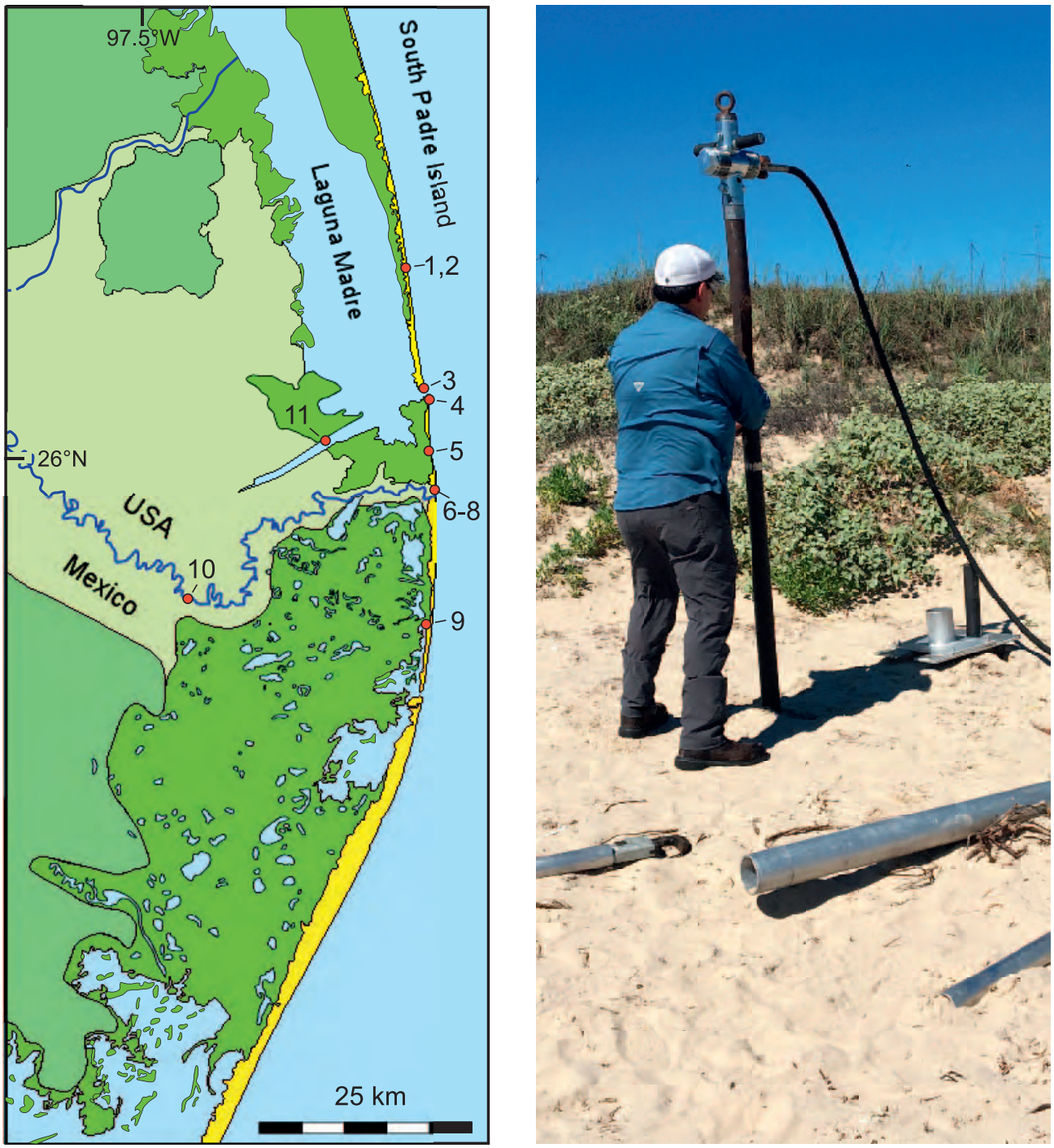

Figure 4. Enlargement of the sample site location map from Figure 2 with a photograph of vibracore sample recovery from South Padre Island–Edwin King County Beach (sample location 1 and 2).

late 1920s. The 27–km long deep-water Brownsville Ship Channel was subsequently dredged inland from Brazos Santiago Pass to Brownsville (Ewing and Gonzalez, 2016). This channel has been steadily deepened throughout the years and is now at 13 m navigation depth (Figure 3).

METHODS

A total of 11 samples were collected. A vibracorer was employed to enable the properties of surface *vs*. deeply buried sand to be contrasted at two separate locations. Sample locations are shown in Figures 3 and 4 with map coordinates

Table 1. *Sample locations and descriptions of the setting in which the samples were collected.*

Sample	Location	Details	Map Coordinates
1	South Padre Island (Edwin King County Park)	top of core	26.18986 N, −97.177481 W
2	South Padre Island (Edwin King County Park)	bottom of core	26.18986 N, −97.177481 W
3	South Padre Island (Isla Blanca Park) near jetty	surface sand	26.07160 N, −97.155961 W
4	Boca Chica Beach (Brazo Santiago Pass)	surface sand	26.06400 N, −97.150400 W
5	Boca Chica Beach (midpoint)	surface sand	26.00180 N, −97.150800 W
6	Boca Chica Beach (near Rio Grande mouth)	surface sand	25.95660 N, −97.147833 W
7	Boca Chica Beach (near Rio Grande mouth)	top of core	25.95660 N, −97.147833 W
8	Boca Chica Beach (near Rio Grande mouth)	bottom of core	25.95660 N, −97.147833 W
9	Mexico–Playa Bagdad	surface sand	25.82382 N, −97.151983 W
10	Rio Grande	river sand	25.84968 N, −97.4357667 W
11	Brownsville Ship Channel	dredged sand	26.01210 N, −97.271050 W

and additional details provided in Table 1. Samples #1 (surface) and #2 (5 m depth) were collected from a vibracore extracted from beach sand at Edwin King County Park, 25 km north of the mouth of the Rio Grande River (Figure 4). A second South Padre Island beach sand (#3) was collected 11 km to the south at Isla Blanca Park near the Brazos Santiago Pass jetty. Three additional beach sands (#4, #5, and #6) were collected along Boca Chica beach between Brazos Santiago Pass and the active mouth of the Rio Grande River. Surface sand (#7) and a 5 m deep vibracore sample (#8) was collected from the active mouth of the Rio Grande (Figure 4). The final sand sample was collected from sediment dredged from the Brownsville ship channel (#11) (Figure 4).

Sand samples were disaggregated, dried, and characterized morphologically at San Diego State University using a CAMSIZER instrument (Blott and Pye, 2001). The CAMSIZER measures both particle size and shape and calculates textural analysis parameters (Blott and Pye, 2001). Sand fed through the CAMSIZER is photographed with two orthogonal high-speed digital cameras. These allow measurement and shape analysis of a wide range of particles from 30 μm to 30 mm.

Zircon ($ZrSiO_4$) is a primary target phase for U-Pb geochronology (*e.g.*, Schoene, 2014). The abundance of detrital zircon in clastic sedimentary rocks, combined with its resistance to chemical and physical weathering, contributes to the popularity and prolificacy of the U-Pb system for geochronology performed with sedimentary rocks (Gehrels, 2012). Because most zircon is igneous in origin, zircon U-Pb ages are generally thought to represent the time at which zircon within a host igneous rock crystallized from magma. Thus, in cases where sediments are directly routed from igneous source regions to the depositional basin, a distribution of detrital zircon ages represents the distribution of crystallization of igneous rocks within the source region (*e.g.*, Gehrels, 2012). While reworking of sediment from previously deposited rocks obscures primary relationships with basement terranes, the detrital zircon age distribution of a sample remains a distinctive property that can be used to characterize sedimentary provenance (*e.g.*, Fletcher *et al.*, 2007; Kimbrough *et al.*, 2015; Malkowski *et al.*, 2020).

Concentrates of detrital zircon were extracted from the suite of Rio Grande delta sands using conventional hydrodynamic, magnetic, and density methods. Zircons were hand-selected with the aid of a binocular zoom microscope. Grains were mounted, potted in epoxy, sectioned, and polished. Uranium-lead isotopic ages were measured by laser ablation, inductively coupled plasma mass spectrometry (LA-ICP-MS) at the Arizona Laserchron Center. Standard Sri Lanka zircon (standard zircon SL with a 564 Ma U-Pb age) (Kimbrough *et al.*, 2015) and secondary standard zircon R33 were added to the mounts to standardize the U-Pb measurements. A total of 647 of the 1106 grains yielded $^{206}Pb/^{238}U$ ages <750 Ma. Since Mesoproterozoic and early Paleoproterozoic zircons have higher and thus more readily measured ^{207}Pb ion intensities, $^{207}Pb/^{206}Pb$ ages were used instead of $^{206}Pb/^{238}U$ ages because the former are generally more accurate for ancient zircons. Approximately 13% percent of the older (>750 Ma) zircons were negatively impacted by U-Pb discordance at the 15% level. Results discordant by greater than 15% were excluded from further analysis.

The Kolmogorov-Smirnov (K-S) test was utilized to calculate the probability that two measured detrital zircon age distributions were derived from the same population (Press *et al.*, 1992). The probability (P) yielded by the test is used to evaluate the null hypothesis that two distributions (A, B) are drawn from the same population. The value of P is calculated from the maximum vertical separation (D) of cumulative age distributions of samples A and B. P also depends upon the sample size (N_e) where $N_e = N_A * N_B/(N_A + N_B)$. A value of $N_e > 25$ is required for a valid test (Press *et al.*, 1992). If $P \geq 0.05$, the null hypothesis is upheld because the age distributions for the two samples are not distinguished at 95% confidence. Alternatively, if $P < 0.05$, the null hypothesis can be rejected. A P value < 0.05 thus indicates that there is a statistically meaningful difference between the age distributions associated with two samples.

The K-S text results reported here were generated using a program written by O.M. Lovera that implements calculations presented in Press *et al.* (1992). Lovera's algorithm calculates P for the case in which experimental error is ignored. This is the conventional K-S test that calculates D from cumulative age distributions (*i.e.* the raw data) and P where experimental error is taken into account. The later calculates D from two cumulative probability density function (*i.e.* error-weighted ages) and yields high values of P.

RESULTS

Table 2 reports the textural attributes of the sand samples investigated (see Table 1). As indicated, most samples were unimodal, well-sorted, fine-grained sand. The term "slightly gravelly" generally refers to trace shell detritus. The detection limit for textural analysis (30 micron) was reached with sample 8.

Table 2. *Textural attributes of sand samples. Most samples were unimodal, well-sorted, fine-grained sand. In many instances, the term "slightly gravelly" refers to trace shell detritus. Note that the detection limit for analysis (35 micron) was reached with sample #8.*

Sample	Geometric Mean (μm)	Logarithmic Mean (ϕ)	Sorting	Skewness	Kurtosis	Sediment Mode/Texture
1	236	2.083	1.238	0.008	1.030	unimodal, very well sorted/sand
2	236	2.084	1.237	0.049	1.044	unimodal, very well sorted/slightly gravelly sand
3	232	2.017	1.314	0.139	1.056	unimodal, well sorted/slightly gravelly sand
4	232	2.017	1.314	0.139	1.056	unimodal, well sorted/slightly gravelly sand
5	235	2.089	1.29	0.096	1.094	unimodal, well sorted/sand
6	241	2.053	1.476	0.254	1.174	unimodal, moderately well sorted/sand
7	225	2.155	1.276	−0.013	1.178	unimodal, well sorted/slightly gravelly sand
8	<40	-	-	-	-	silt
9	225	2.155	1.273	0.115	1.134	unimodal, very well sorted/slightly gravelly sand
10	219	2.192	1.369	−0.027	1.161	unimodal, well-sorted/slightly gravely sand
11	228	2.213	1.325	0.065	1.045	unimodal, well-sorted/sand

Figure 5 illustrates the cumulative U-Pb zircon age distributions measured from the sample suite. Two samples (Playa Bagdad and the Brownsville Ship Channel) yield age distributions that bracket the distributions yielded by all other samples. The modern sand from the Rio Grande River is also emphasized for reference. The modern sand from Playa Bagdad may represent a less disturbed part of the delta system in northeastern Mexico. Finally, the Brownsville Ship Channel sample may expose older (*i.e.* pre-Holocene) sediments.

The U-Pb detrital zircon age distributions of the Rio Grande River, Playa Bagdad, and Brownsville Ship Channel are shown in Figure 6 as probability density functions. As indicated, all three distributions reveal similar age maxima with abundant Cenozoic and Mesozoic U-Pb ages and a broad distribution of Neoproterozoic, Mesoproterozoic, and Paleoproterozoic zircon. The largest age maxima occur between 40–20 Ma (Figure 6). Because the age peaks for all three samples are rather similar, the cumulative probability density functions (Figure 5) best illustrate the overall differences between the samples. As indicated, the Playa Bagdad sample has 70% < 250 Ma zircon while the Rio Grande and Brownsville ship channel samples have 52% and 42%, respectively, of grains <250 Ma.

Age distributions measured from the eight beach sand samples (#1–#8) including the two borehole samples (#2 and #8) are dispersed around the age distribution for the Rio Grande sample (#10) (Figure 5). Table 3 presents 2–sample K-S test results from the eleven samples. As indicated, beach sand samples #1–#8 are statistically indistinguishable from Rio Grande river (#10) at 95% confidence. In contrast, comparison of the Playa Bagdad, Mexico sample (#9) with the Rio Grande River sample (#10) yields a value of $P = 0.03$ (measurement error neglected). This indicates that the Playa Bagdad sample

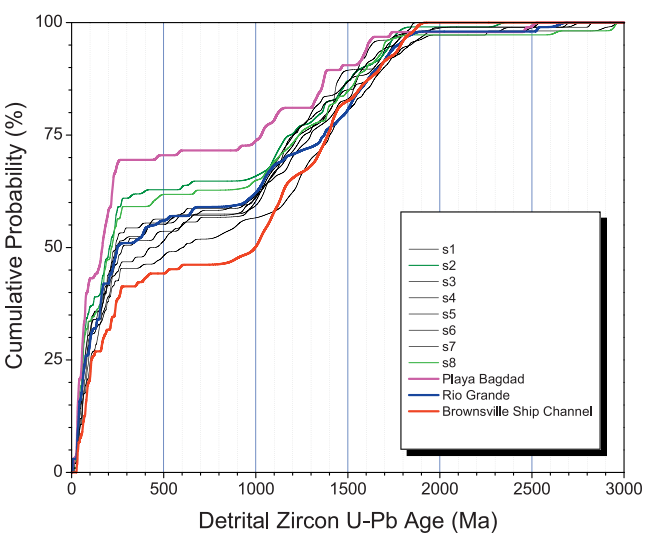

Figure 5. Cumulative plot of detrital zircon U-Pb age distributions for all Rio Grande delta modern sand samples. Results from Playa Bagdad in Mexico and the Brownsville ship channel bound all other results and serve as end members for future analysis. Rio Grande modern river sand is also used as a reference in future calculations.

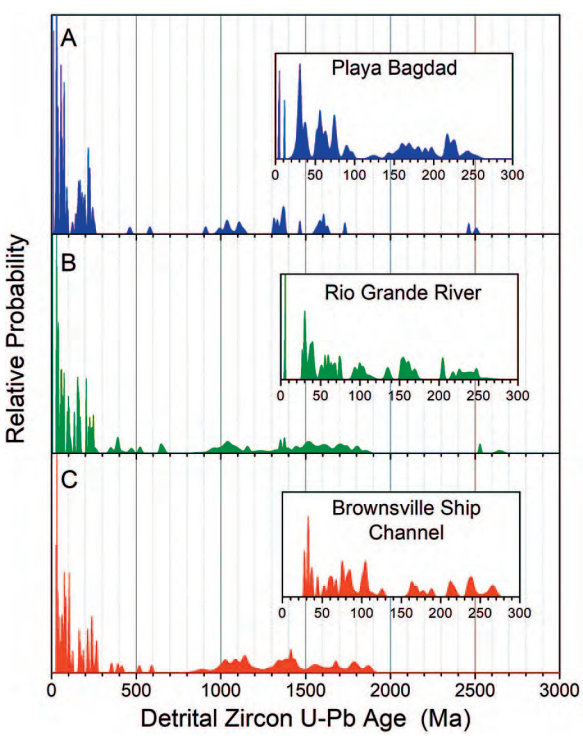

Figure 6. Representative probability density functions of detrital zircon 0–3000Ma U-Pb age distributions measured from modern sand end members: (A) Playa Bagdad (Mexico); (B) Rio Grande; (C) Brownsville ship channel. Insets provide finer detail for 0–300 Ma portion of distribution.

Table 3. *Results of the two-sample, Kolmogorov-Smirnov (K-S) test. All comparisons are made relative to sample #10 (Rio Grande sand). A probability (*P*) of 0.05 or greater means that the two distributions cannot be distinguished at 95% confidence. Calculations performed with the raw data only compare the cumulative distribution functions of two samples. This is the conventional K-S test. Error-weighted K-S results compare the probability density functions (PDF) of the two samples. Because the PDF's are smoothed, calculated values of* P *are higher.*

Sample		Error-Weighted Data		Unweighted Data	
	N	D_{raw}	P_{raw}	$D_{weighted}$	$P_{weighted}$
1	94	0.075	0.937	0.084	0.873
2	105	0.107	0.573	0.109	0.552
3	97	0.097	0.727	0.107	0.603
4	92	0.043	1.000	0.053	0.999
5	103	0.087	0.823	0.096	0.722
6	108	0.103	0.614	0.116	0.464
7	98	0.070	0.961	0.077	0.923
8	110	0.081	0.868	0.081	0.869
9	95	0.196	0.041	0.203	0.031
10	**100**	**0.000**	**1.000**	**0.000**	**1.000**
11	104	0.128	0.347	0.131	0.326

is statistically resolved. Additional K-S tests performed indicate that samples #2, #4, #5, #7, and #8 are statistically indistinguishable at 95% confidence from the Playa Bagdad sample (#9). Samples #2 ($P = 0.37$) and #8 ($P = 0.30$) are most similar to the Playa Bagdad sample (#10). Comparisons made between the Brownsville Ship Channel dredged sand (#11) reveal that six of the eight samples overlap at 95% confidence.

DISCUSSION

The Rio Grande delta was a fluvial-dominated system that carried coarse sand and gravel between *ca*. 8000 and 3000 years ago during the Holocene Climatic Optimum (Rodriguez, Fassell, and Anderson, 2001). Today, dams, irrigation projects, and other factors have water reduced flow within the Rio Grande to the extent that the river carries only fine sand and no longer consistently flows to the Gulf Coast (Anderson *et al*., 2014; Benke and Cushing, 2005; Jepsen *et al*., 2003). This stark contrast in conditions prompts the following questions: (1) Is there a contrast in the provenance signature of Rio Grande River sand that can be attributed to dam construction?; (2) Is modern sand proximal to the mouth of the Rio Grande River primarily being supplied by the Rio Grande River or from northeast-directed longshore sediment along the modern shoreline of the Gulf of Mexico?

How Have Dams Affected the Provenance of Sand within the Delta?

Dams disrupt the continuity of sediment transport along rivers. Over the past decade, sediment trapping caused by dam construction has caused 85% of the deltas worldwide to experience severe flooding, submergence, and other adverse effects (Nienhuis *et al*., 2020; Syvitski *et al*., 2009). The gravitational potential energy possessed by water released downstream from newly constructed dams works to rapidly remove pre-existing bedload (Kondolf, 1997). For example, construction of Glen Canyon Dam along the Colorado River in northern Arizona caused the downstream channel to incise, armor, and narrow (Grams, Schmidt, and Topping, 2007). More locally, construction of Livingston Dam along the Trinity River in central Texas caused bed erosion 50–60 km downstream of the dam (Smith and Mohrig, 2017). This included lowering of the channel bed, reduction in the sediment volume of channel bars, coarsening of sediment on bar tops, steepening of channel banks, and reduction in lateral migration rates of river bends (Smith and Mohrig, 2017).

Falcon Dam (volume of 3×10^9 m^3) was completed in 1954 and represents the last major dam on the Rio Grande (Moya *et al*., 2016). Further downstream, the last major tributary to the Rio Grande, the Rio San Juan, is dammed 20 km upstream from its confluence with the Rio Grande (Figures 1 and 2). Marte R. Gómez Reservoir (surface area of 235 km^2) has been in place since 1936. Erosion of the riverbed has occurred downstream of these two dams since their construction. Moreover, additional sediment is contributed from the topographically elevated region surrounding the dams. Extensive dissection of the landscape near the reservoirs has formed arroyos that lead to the Rio Grande River (Figure 2). The area of maximum relief near Falcon and Marte R. Gómez Dams is underlain by Eocene, Oligocene, and Miocene strata (Page, VanSistine, and Turner, 2005) (Figure 2). Up to *ca*. 125 meters of relief occurs in the region adjacent to Falcon and Marte R. Gómez Dams (Figure 2). Sandstones are characteristically enriched in zircon (*e.g*., Garcon *et al*., 2014) and are generally readily eroded when weakly cemented (Small *et al*., 2015). Further downstream, near Rio Grande City and the furthest downstream Miocene outcrops, the amount of local relief has decreased to *ca*. 60 meters. By the time the Rio Grande River reached Reynosa, topography is muted and the flood plain of the Rio Grande delta expands radially (Figure 2). Further south, the Rio Grande transitions to an aggregational form with super-elevated levees relative to the floodplain.

To test whether post-1954 erosion of sedimentary rocks south of Falcon Dam has altered the detrital zircon provenance signature of the Rio Grande River sand within the delta region, relevant data from past studies was evaluated. Figure 7 compares the results of previous detrital zircon studies performed with Rio Grande river sand upstream of the reservoir. Blum *et al*. (2017) and Fan, Brown, and Li (2019) independently collected and measured modern Rio Grande River detrital zircon U-Pb age distributions from near the city of Laredo, Texas, about 115 upstream of Falcon Dam (Figure 1). These are shown in Figures 7B and 7C, respectively. The primary distinction between the two Laredo samples and Brownsville (this study) is the much higher proportion of 40–20 Ma zircon in the former.

The cumulative age distributions for all three samples are shown in Figure 7D. The two independently collected and analyzed samples from Laredo (Blum *et al*., 2017; Fan, Brown, and Li, 2019) are indistinguishable within 95% confidence ($P = 0.86$). In contrast, comparisons of the Blum *et al*. (2017) and Fan, Brown, and Li (2019) samples from above Falcon Dam with the Rio Grande River sample from Brownsville (this study) yield P values (4×10^{-7} and 6×10^{-5}, respectively). These results indicate that the downstream sample from Brownsville is statistically distinguished from both upstream samples at 95% confidence. The cumulative age distributions of the Laredo Rio Grande samples plot above the envelope defined by all results from this study (compare Figures 5 and 7). The Playa

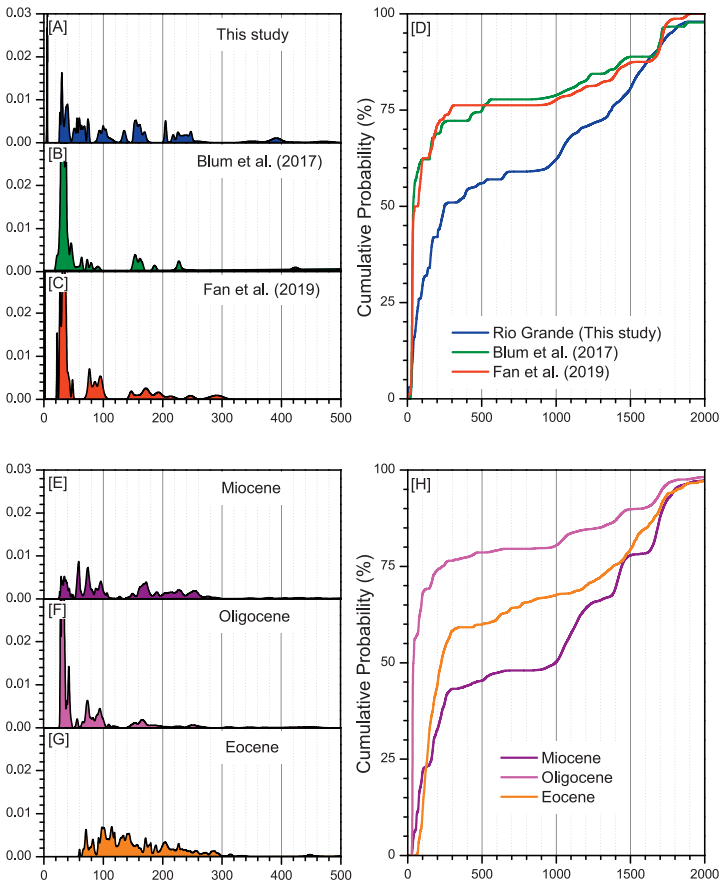

Figure 7. Detrital zircon U-Pb age distributions from modern sand and Cenozoic sedimentary rocks discussed in the text: (A) modern Rio Grande river sand collected near Brownsville, Texas (this study); (B) modern Rio Grande river sand collected near Laredo, Texas reported by Blum *et al*. (2017); (C) modern Rio Grande river sand collected near Laredo, Texas reported by Fan, Brown, and Li (2019); (D) Cumulative age distributions from samples A–C.; (E) Pooled age distribution for Miocene strata constructed from Fan, Brown, and Li's (2019 samples #5–#7, and Xu, Stockli, and Snedden's (2017) samples GOM 2–4); (F) Pooled age distribution for latest Eocene-Oligocene strata based upon Fan, Brown, and Li's (2019) samples #1–#4, and Blum *et al*.'s 2017 GOM 58 sample; (G) Pooled age distribution for south Texas late Paleocene–earliest Eocene upper Wilcox Group samples Z2, Z3, Z6, Z8 from Mackey, Horton, and Milliken (2012); and (H) Cumulative age distributions from pooled sampled in E–G.

Bagdad sample (#9) and the two vibracore samples (#2, #8) from the present study plot closest to the Laredo Rio Grande river sand samples. While these three samples (#2, #8, and #9) appear are likely to be the most pristine samples in the suite, all are distinguishable at 95% confidence from Blum *et al*.'s (2017) and Fan, Brown, and Li's (2019) Rio Grande samples.

The similar sample preparation and laboratory procedures were used to generate all three data sets argues against analytical issues as a cause for the significant difference between the Brownsville and Laredo river sands from the Rio Grande (Figure 7E–G). Interruption of downstream sediment transport as a result of dam construction provide a much more likely explanation. In a systematic study of the impact of dams upon downstream propagation of sediment and detrital zircon U-Pb age distributions, Malkowski *et al*. (2020) argued that the mass of sediment transported by California's Sacramento-San Joaquin River to the Sacramento Delta was sufficiently large prior to dam construction to mitigate against bias caused by sediment trapped in dams. However, this conclusion requires that volumetrically significant new sources of sediment do not appear downstream of the dam after the reservoir is filled.

Figure 7E–G displays representative detrital zircon age distributions from Eocene, Oligocene, and Miocene strata from southern Texas (Fan, Brown, and Li, 2019; Mackey, Horton, and Milliken, 2012; Xu, Stockli, and Snedden, 2017). Each distribution represents 4–6 pooled samples collected from southwestern Texas (see compilation details in Fan, Brown, and Li, 2019). The cumulative age distributions are shown in Figure 7H. All are distinguished at 95% confidence from each other and the modern Rio Grande River sand collected from the delta area near Brownsville.

The Eocene distribution is indicated to most strongly resemble the age distribution of the modern Rio Grande River sand (Figure 7H). The Miocene cumulative age distribution plots below both the Eocene distribution and modern Rio Grande River sand, while the Oligocene age distribution plots well above it (Figure 7H). Interestingly, the Oligocene age distribution strongly resembles the age distributions of both

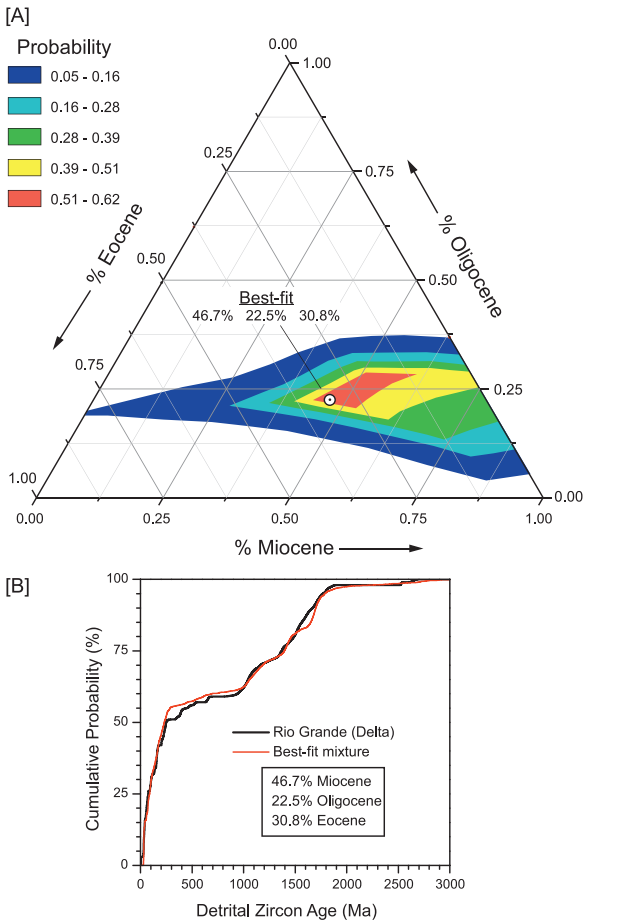

Figure 8. Results of ternary mixing calculations performed with Cenozoic strata displayed in Figure 7 to replicate the Rio Grande modern sand from the delta region (sample 10 from this study): (A) Ternary plot. Contours represent constant values of probability calculated from an extended form of the K-S statistic (see text for further details). Filled contours represent regions of ternary space where $P \geq 0.05$. All mixtures above this threshold are statistically indistinguishable Rio Grande age distribution from the delta region. Best-fit composition is shown; (B) Cumulative probability plot illustrating model fit to measured Rio Grande age distribution.

modern Rio Grande River sand collected in Laredo, above Falcon Dam (Figure 7). When the K-S test is applied using the Oligocene age distribution as the comparison, P values of 0.15 and 0.26 are obtained for the Fan, Brown, and Li (2019) and Blum *et al*. (2017) modern Rio Grande River sands from the Laredo area.

Rigorous assessment of the ability of postdam sediment eroded from Early Cenozoic bedrock downstream from Falcon and Marte R. Gómez Dams to dilute the Oligocene zircon rich sand provenance signature reported for the modern Rio Grande near Laredo (Blum *et al*., 2017; Fan, Brown, and Li, 2019) (Figure 7B,C) to that measured near Brownsville (this study; Figure 7A) requires knowledge of both the mass and zircon concentration of reworked predam and newly eroded postdam sediment within the Rio Grande delta. While this mass balance calculation is beyond the scope of the present study, a simpler question can be posed: In the absence of any pre-existing river sediment, is it possible to mix the detrital zircon age distributions representing Eocene, Oligocene, and Miocene strata below the two dams in a manner that reproduces the modern Rio Grande river sand from Brownsville? To answer this, three-component mixing calculations were performed.

The mixing calculations presented below employ an extended form of the K-S statistic developed by O.M. Lovera that is applicable to mixtures of age distributions (see Kimbrough *et al*., 2015). The intersectional probability approach employed assumes that each component to the mixture (*i.e*. each age distribution) is independent from the other two. Ternary mixtures were calculated with a resolution of 0.1%. Results of these calculations are portrayed in Figure 8A. All mixtures that are indistinguishable from modern Rio Grande River sand (*i.e*. yield $P > 0.05$) are contoured. The "best fit" solution that corresponds to the highest P value is 46.7% Miocene, 22.5% Oligocene, and 30.8% Eocene. Note however, that 28% of all ternary mixtures calculated were indistinguishable at 95% confidence from the age distribution yielded by modern Rio Grande River sand (Figure 8A). For example, any mixture between 95% Miocene–5% Oligocene and 63% Miocene–37% Oligocene on the Miocene–Oligocene binary join has a P value above 0.05. A more restricted range of acceptable mixtures centered on 80% Eocene–20% Oligocene occurs along the Eocene–Oligocene ternary join. In ternary space, a wedge shaped swath of acceptable mixtures trends parallel to, but does not intersect, the Eocene-Miocene binary join.

The significance of these mixing calculations depends upon how representative the input age distributions are for Cenozoic strata that crop out below Falcon and Marte R. Gómez Dams. Available data indicate that the age distributions used are highly reproducible as a function of geologic time throughout southern Texas (Blum *et al*., 2017; Fan, Brown, and Li, 2019; Mackey, Horton, and Milliken, 2012; Xu, Stockli, and Snedden, 2017). Assuming that the age distributions used in the calculations are representative, it can be concluded that the present-day detrital zircon U-Pb age provenance signature of the modern Rio Grande River can be accounted for by sand locally eroded from Early Cenozoic strata.

Have Longshore Currents Transported Sand from Southern Mexico to the Rio Grande Delta?

Sediment dispersal within marine delta systems is influenced by geological setting, sediment flux, and particle size distribution, and a host of hydrodynamic processes acting along the river/ocean interface (Masselink and Hughes, 2003; Woodroffe, 2002). Long-term coastal subsidence/emergence as a result of sea level variation has a major impact upon deltaic systems (Allen, 1965). Fluvially dominated deltas form when sediment input overwhelms wave energy and are more prevalent during periods of low sea level (Komar, 1973; Seybold, Andrade, Jr., and Herrmann, 2007). Alternatively, wave-dominated delta configurations involving barrier island formation occur when river sediment flux is reduced and/or wave energy becomes sufficiently high to winnow away fine-grained sediment and redistribute river sand along the shoreline (Nienhuis, Ashton, and Giosan, 2015; Seybold, Andrade, Jr., and Herrmann, 2007).

A Late Holocene reduction in sediment supply caused the Rio Grande delta to become a wave-dominated system ringed by barrier islands (Rodriguez, Fassell, and Anderson, 2001) (Figure 2). Depending upon the effectiveness of long-shore transport, it is conceivable that sand within the barrier islands of the Rio Grande could contain extraregional sand derived from southern Mexico. The efficacy of long distance sand transport by littoral currents during sea level highstands depends upon the width of the continental shelf, the steepness of the littoral zone, and whether or not topographic barriers exist (Ribó *et al.*, 2020). In cases where rising sea level broadens the shelf, the possibility of far-traveled sediment transport via long-shore drift is enhanced since less sand is diverted offshore. For example, Garzanti *et al.* (2017) have employed detrital zircon age distributions and other provenance data to trace an 1800 km long littoral zone sand highway that extends from the Orange River of coastal Namibia to Angola along Africa's Atlantic coastline. Less laterally extensive (800–1000 km scale) longshore transport has also been documented along southern Brazil's Atlantic coast (Calliari and Toldo, 2016) and along the Pacific shore of Australia (Boyd *et al.*, 2008).

Recognition of extraregional sediment requires distinctive age components. There are two distinctive provenance signatures represented along the Tamaulipas-Veracruz Gulf Coast (Figure 1) that are potentially useful for detecting extraregional sand in the Rio Grande barrier islands. Beach sand directly sourced from the Trans Mexican volcanic belt (Figure 1) contains significant proportions of diagnostic Quaternary detrital zircon (Armstrong-Altrin *et al.*, 2018; Ramos-Vázquez and Armstrong-Altrin, 2019) (Figure 9). For example, nearly 50% of the detrital zircon age population examined from beach sand collected along the southern Veracruz coast near the mouth of the Rio Papaloapan (Figure 1) are <10 Ma with most grains yielding Quaternary U-Pb ages (Alvarado Beach) (Armstrong-Altrin *et al.*, 2018) (Figure 9). The inset in Figure 9 documents the Quaternary-rich character of zircon present within six samples from the southern Vera Cruz coast (Armstrong-Altrin *et al.*, 2018; Ramos-Vázquez and Armstrong-Altrin, 2019) (locations shown in Figure 1).

The basement of south-eastern Mexico is dominated by Triassic-Permian, early Paleozoic–late Neoproterozoic, and Grenville age zircon (Centano-Garcia, 2017) (Figure 1). The magenta (200–300 Ma), cyan (400–700 Ma), and yellow bands (900–1150 Ma) in Figure 9 demonstrate coastal samples collected along the southern Vera Cruz coast are enriched in zircon in these age ranges. For example, the combined Rio Girijalva and Rio Usumacinta collectively drain the Chiapas Massif and Oaxacan complexes of southern Mexico (Figure 1). The Atasta beach sample of Armstrong-Altrin *et al.* (2018) is highly enriched in early Paleozoic–late Neoproterozoic and Grenville zircon (Figure 9). Additional detrital zircon samples from the Bosque and Paseo del Mar coastal areas also contain these age components (Ramos-Vázquez and Armstrong-Altrin, 2019) (Figures 1 and 9).

To test for southern Mexican (*i.e.* Vera Cruz coast) provenance in the barrier island sand of the Rio Grande delta, a composite age distribution was constructed by pooling all barrier island samples (#1–#8) from the present study (Figure 9). This is justified because all are indistinguishable at 95% confidence by the K-S test. Figure 9 indicates that while Pliocene zircon is present in the composite sample, the details of the youngest portion of the composite age distribution (samples #1–#8) does not conform to the age distribution of the Trans Mexican volcanic belt. The inset to Figure 9 shows the youngest (0–50 Ma) detrital zircon present in the Alvarado beach sands and the composite sample (#1–#8) from the Rio Grande delta. Only 13 of the 807 analyses from the eight beach sand samples yielded ages in the 10–0 Ma range. Moreover, the 10 of the 13 young analyses clustered at 4.8 ± 0.5 Ma. Zircon sampled from the Trans Mexican volcanic belt is expected to yield abundant Quaternary zircon. The 1.6% levels of 10–0 Ma zircon present in the composite Rio Grande beach sand (#1–#8) are comparable to the background levels of this age zircon within the Rio Grande system (Blum *et al.*, 2017; Fan, Brown, and Li, 2019) (Figure 7).

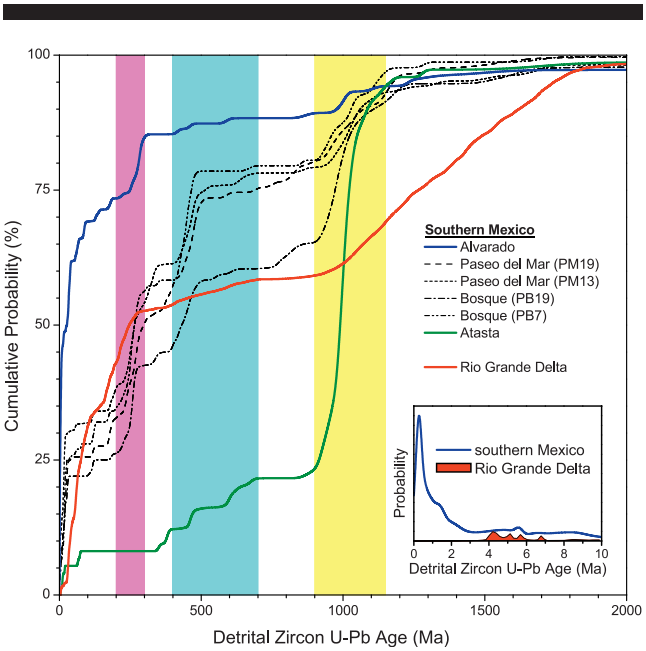

Figure 9. Results of model simulation of coastal currents along the Mexican (Tamaulipas-Veracruz) Gulf Coast reported by Zavala-Hidalgo, Morey, and O'Brien (2003) based upon seven years of model data. Calculations simulate the entire Gulf of Mexico and are based upon the Navy Coastal Ocean Model (Martin, 2000), and are forced with climatological monthly surface fluxes of heat and momentum derived from the Comprehensive Ocean Atmosphere Data Set (DaSilva, Young, and Levitus, 1994); (A) Model predictions each month for 26° N (Rio Grande delta); (B) 24° N (Tamauilpas coast); (C) 22° N (Ciudad Madero); (D) 20° N (Veracruz coast); (E) Map of predicted surface current velocities for the western Gulf of Mexico for June; (F) Map of predicted surface current velocities for the western Gulf of Mexico for December.

Similarly, the provenance signature of the composite (#1–#8) age distribution also contrasts markedly with that from the basement of southeastern Mexico (Figure 9). Specifically, the proportions of early Paleozoic–Latest Neoproterozoic (400–700 Ma) and Grenville (900–1150 Ma) are much lower than is the case for the coastal areas of southern Mexico (Figure 9). Hence, no compelling evidence exists from the Rio Grande delta samples investigated in this study for northward longshore

transfer of sediment from as far south as the Vera Cruz coast of southern Mexico.

Tapia-Fernandez, Armstrong-Altrin, and Selvaraj (2017); Hernandez-Hinojosa *et al*. (2018), Armstrong-Altrin *et al*. (2018), and Ramos-Vázquez and Armstrong-Altrin (2019) have all concluded on the basis of detrital zircon age systematics and other compositional attributes of coastal sediment that river supplied sediment to the coastal areas was much more important in defining the provenance and composition of coastal sediments than offshore factors such as longshore currents.

Further north, the nature of longshore sediment transport along the Mexican (Tamaulipas-Veracruz) Gulf Coast is less well understood. The Mexican coastal shelf is considerably narrower than the Texas shelf and is thus more vulnerable to sediment diversion to deeper water (Figure 1). At the latitude of Brownsville, prevailing SE winds intersect the nearly N-S trending south Texas coastline at an acute angle and cause coastal longshore transport to be predominately directed to the north (Shideler, 1978). Numerical simulations performed by Zavala-Hidalgo, Morey, and O'Brien (2003) are presented in Figure 10. The calculations simulate the entire Gulf of Mexico, are based upon the Navy Coastal Ocean Model (Martin, 2000), and are forced with climatological monthly surface fluxes of heat and momentum derived from the Comprehensive Ocean Atmosphere Data Set (DaSilva, Young, and Levitus, 1994). The results indicate that the Tamaulipas-Veracruz shelf experiences a swift seasonal reversal of the along-shelf current (Figure 10). Littoral currents run down the coast from September to March and up the coast from May to August.

Coastal observations confirm that seasonal variation in the direction of longshore current occurs along the Veracruz shelf (Figure 1). For example, net sediment transport in the Rio Nautla area of Veracruz, Mexico is indicated to occur from south to north on the basis of northward prograding sand spits and river-mouth bars (Self, 1977) (Figure 1). During the winter however, winds out of the NE cause longshore current to flow in the opposite direction. The Rio Tecolutla and the Rio Nautla both drain the Late Miocene–Holocene Trans Mexican Volcanic belt and carry abundant volcanic detritus and distinctive limestone lithoclasts. Self (1977) reports that lithoclasts supplied by the Rio Tecolutla and Rio Nautla derived are transported as far as 60 km south of the Rio Nautla during the winter reversals.

A significant barrier to longshore transport occurs at Cabo Rojo (21.5° N) on the Veracruz coast, 150 km north of the Rio Nautla (Figure 1). Stapor (1971) has described the impact of the barrier reef complex at Cabo Rojo. Three reefs (Arrecife Blanquila, Arrecife Medio, and Isla De Lobos) occur along 100° south bearing that extends 5 to 12 km off the coast. These reefs have facilitated development of a lagoon (Laguna de Tamiahua) in their lee that deflects the coastline up to 25 km east of the regional trend. The overall geometry of the cape barrier is that of an asymmetric tombolo with a 60 km northern leg and a 35 km southern leg developed landward of the Blanquilla-Lobos coral reef tract (Stapor, 1971). This perturbation of the coastline serves to direct either north- or south-flowing shelf sand into deeper water (Stapor, 1971).

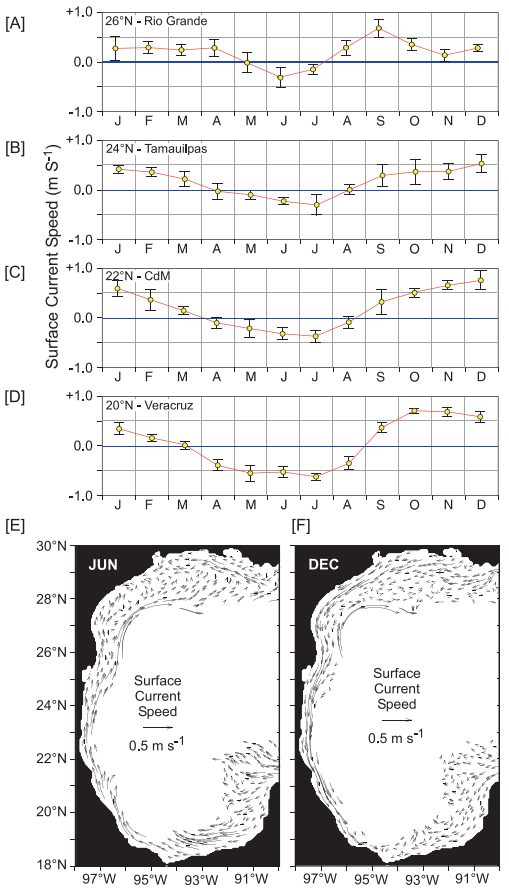

Figure 10. Cumulative probability plot of detrital zircon U-Pb age distributions discussed in the text. Data from the Alvarado and Atasta Beach areas of the Veracruz coast of Mexico is from Armstrong-Altrin *et al*. (2018). The Alvarado beach sample represents sediment carried by the Papaloapan River which drains the adjacent Trans Mexican volcanic belt (see Figure 1). Note that 50% of the age distribution is defined by 10–0.25 Ma volcanic zircon. The Atasta Beach sample represents sediment delivered from the Rio Girijalva and Rio Usumacinta that collectively drain the Chiapas Massif and Oaxacan complexes of southern Mexico. A pooled age distribution constructed from samples #1–#8 (this study) is shown for comparison. Note that the cumulative age distributions of the Atasta and Rio Grande samples differ dramatically. The inset shows that Rio Grande delta sands do not contain any resolvable volcanic zircon from the Trans Mexican volcanic belt.

Sediment transport off of the shelf in this region may be further amplified by periodic collisions of anticyclonic loop current rings against the 21.5° to 23° N segment of the Mexican continental margin (*e.g*., Vidal, Vidal, and Perez-Molero, 1992). These interactions are thought to occur with a high enough frequency to serve as the most effective mechanism to transfer continental shelf water (and presumably shelf sediment) into the deeper gulf (Vidal, Vidal, and Perez-Molero, 1992). Further north Stapor (1971) concluded that the morphology of barrier islands along the southern (Tamaulipas) part of the Rio Grande delta indicate net southward longshore transport. This implies that south-directed flow in the seasonal variation in littoral

currents shown in Figure 10 prevails over north-direct transport.

In summary, available evidence indicates that factors including the narrow Veracruz-Tamaulipas continental shelf, geomorphic features (*e.g*., Cabo Rojo), oceanographic phenomena (*e.g*., ring current collisions with the shelf), and seasonal variation in the direction of wind-driven littoral currents (Figure 10) all support Stapor's (1971) conclusion that coast-parallel sediment transport is presently highly compartmentalized along the Veracruz-Tamaulipas Gulf Coast. This conclusion agrees with that of Armstrong-Altrin *et al*. (2018) that sediment supplied by major rivers is far more important than longshore currents in determining the provenance and composition of Late Holocene coastal sediments along the Veracruz-Tamaulipas Gulf Coast.

CONCLUSIONS

Detrital zircon U-Pb age distributions were measured from a variety of modern sediments from the Rio Grande delta of southern Texas, U.S.A. and northern Tamaulipas, Mexico in order to detect and quantify the potential impacts of dam construction and longshore transport.

Modern Rio Grande River sand yields a detrital zircon U-Pb age distribution that is statistically indistinguishable from six surface beach sands collected along the barrier islands of the Rio Grande delta. The Playa Bagdad, Mexico sample appears distinct from the Rio Grande River sample in that it is enriched in Oligocene (notably 40–20 Ma) zircon. Similarly, two 5 meter deep vibracore samples of beach sand are similarly enriched in this component. These three samples may represent the most pristine delta deposits in the suite.

A statistically meaningful contrast in detrital zircon provenance signature exists between two independently reported Rio Grande modern sand samples collected upstream from Falcon Dam near Laredo, Texas and the sample collected in this study near Brownsville, Texas in the delta region. The former is highly enriched in Oligocene zircon and indistinguishable from one another at 95% confidence. The samples upstream from Falcon Reservoir most strongly resemble the Playa Bagdad and 5 meter vibracore samples from this study.

Ternary mixing calculations of age distribution representative of Eocene, Oligocene, and Miocene sandstones that crop out below Falcon dam demonstrate that locally eroded material can reproduce the provenance signature of Rio Grande modern sand in the delta. While more rigorous mass balance calculations are required, it is tentatively concluded that the Rio Grande delta sediment that was analyzed contains a large proportion of locally eroded material.

The late Holocene highstand of sea level makes it possible for the wave dominated delta to receive extraregional input via longshore transport. Analysis of available data bearing upon longshore currents along the Tamaulipas Gulf Coast of Mexico indicated the possibility that extraregional sediment could be transported northwards from as far south as the Cabo Rojo area, 420 km to the south. However, analysis of Rio Grande delta beach sands failed to detect meaningful concentrations of distinctive Trans Mexican volcanic belt–derived zircon that would confirm longshore transport on such a scale. This may imply that seasonally variable sand movement along the Mexican (Tamaulipas) Gulf coast is dominated by south-directed littoral currents.

ACKNOWLEDGMENTS

Joan Kimbrough (SDSU) is thanked for assisting with Camsizer analysis at San Diego State University and the UA staff of the Arizona Laserchron Center for help with detrital zircon U-Pb analysis. Oscar Lovera (UCLA) provided codes for calculating Kolmongorov-Smirnoff statistics for individual samples and ternary mixing calculations. Andres Cardenas is thanked for help with sample collection. The four anonymous reviewers are thanked for their thoughtful feedback and suggestions.

LITERATURE CITED

Allen, J.R.L., 1965. Late quaternary Niger Delta, and adjacent areas: Sedimentary environments and lithofacies. *Bulletin of American Association of Petroleum Geologists*, 49(5), 547–600.

Anderson, J.B.; Wallace, D.J.; Simms, A.R.; Rodriguez, A.B., and Milliken, K.T., 2014. Variable response of coastal environments of the northwestern Gulf of Mexico to sea-level rise and climate change: Implications for future change. *Marine Geology*, 352, 348–366.

Armstrong-Altrin, J.; Ramos-Vázquez, M.; Zavala-León, A., and Montiel-García, P., 2018. Provenance discrimination between Atasta and Alvarado beach sands, western Gulf of Mexico, Mexico: Constraints from detrital zircon chemistry and U-Pb geochronology. *Geological Journal*, 53(6), 2824–2848.

Banfield, L.A. and Anderson, J.B., 2004. Late quaternary evolution of the Rio Grande delta: Complex response to eustasy and climate change. *In:* Anderson, J.B. and Fillon, R.H. (eds.), *Late Quaternary Stratigraphic Evolution of the Northern Gulf of Mexico Margin. Society of Sedimentary Research*, Special Publication No. 79, pp. 289–306.

Benke, A.C. and Cushing, C.E., 2005. *Rivers of North America*. Amsterdam: Elsevier Academic Press, 1186p.

Blott, S.J. and Pye. K., 2001. GRADISTAT: A grain size distribution and statistics package for the analysis of unconsolidated sediments. *Earth Surface Processes and Landforms*, (11), 1237–1248.

Blum, M.D.; Milliken, K.T.; Pecha, M.A.; Snedden, J.W.; Frederick, B.C., and Galloway, W.E., 2017. Detrital-zircon records of Cenomanian, Paleocene, and Oligocene Gulf of Mexico drainage integration and sediment routing: Implications for scales of basin-floor fans. *Geosphere*, 13(6), 2169–2205.

Boyd, R.; Ruming, K.; Goodwin, I.; Sandstrom, M., and Schröder-Adams, C., 2008. High stand transport of coastal sand to the deep ocean: a case study from Fraser Island, southeast Australia. *Geology*, 36(1), 15–18.

Calliari, L.J. and Toldo, E.E., 2016. Ocean beaches of Rio Grande do Sul. *In*: Short, A.D. and Klein, A.H.D.F. (eds.), *Brazilian Beach Systems*. Switzerland: Springer, pp. 507–541.

Centano-Garcia, E., 2017. Mesozoic tectono-magmatic evolution of Mexico: An overview. *Ore Geology Reviews*, 81, 1035–1052.

Clark, P.U.; Dyke, A.S.; Shakun, J.D.; Carlson, A.E.; Clark, J.; Wohlfarth, B.; Mitrovica, J.X.; Hostetler, S.W., and McCabe, A.M., 2009. The last glacial maximum. *Science*, 235, 710–714.

Curray, J.R., 1960. Sediments and history of Holocene transgression, continental shelf, northwestern Gulf of Mexico. *In*: Shepard, F.P.; Phleger, F.B., and van Andel, T.H. (eds.), *Recent Sediments, Northwestern Gulf of Mexico*. Tulsa, Oklahoma: American Association of Petroleum Geologists, pp. 221–266.

DaSilva, A.; Young, A.C., and Levitus, S., 1994. *Atlas of Surface Marine Data*. Silver Spring, Maryland: National Oceanic and Atmospheric Administration. https://www.nodc.noaa.gov/OC5/ASMD94/pr_asmd.html

Davis, R.A., 2017. Sediments of the Gulf of Mexico. *In*: Ward, C.H. (ed.), *Habitats and Biota of the Gulf of Mexico: Before the*

Deepwater Horizon Oil Spill. New York: Springer Nature, pp. 165–216.

Ewing, T.E. and Gonzalez, J.L., 2016. The late quaternary Rio Grande delta—A distinctive, underappreciated geologic system. *Gulf Coast Association of Geological Societies Transactions*, 66, 169–180.

Ewing, T.E., 1986. Structural styles of the Wilcox and Frio growth fault trends in Texas: Constraints on geopressured reservoirs. *Bureau of Economic Geology Report of Investigations*, 154, 86p.

Ewing, T.E., 1997. *Tectonic Map of Texas*. Austin, Texas: Bureau of Economic Geology, University of Texas, Austin, scale 1:750,000.

Fan, M.; Brown, E., and Li, L., 2019. Cenozoic drainage evolution of the Rio Grande paleoriver recorded in detrital zircons in South Texas. *International Geology Review*, 61(5), 622–636.

Fletcher, J.M.; Grove, M.; Kimbrough, D.L.; Lovera, O.M., and Gehrels, G.E., 2007. Ridge-trench interactions and the Neogene tectonic evolution of the Magdalena Shelf: Insights from detrital Zircon U-Pb ages from the Magdalena fan and adjacent areas. *Geological Society of America Bulletin*, 119(11–12), 1313–1336.

Galloway, W.E.; Whiteaker, T.L., and Ganey-Curry, P., 2011. History of Cenozoic North American drainage basin evolution, sediment yield, and accumulation in the Gulf of Mexico basin. *Geosphere*, 7(4), 938–973.

Garcon, M.; Chauvel, C.; France-Lanord, C.; Limonta, M., and Garzanti, E., 2014. Which minerals control the Nd–Hf–Sr–Pb isotopic compositions of river sediments? *Chemical Geology*, 364, 42–55.

Garzanti, E.; Dinis, P.; Vermeesch, P.; Ando, S.; Hahn, A.; Huvi, J.; Limonta, M.; Padoan, M.; Resentini, A.; Rittner, M., and Vezzoli, G., 2017. Sedimentary processes controlling ultralong cells of littoral transport: Placer formation and termination of the Orange sand highway in southern Angola. *Sedimentology*, 65(2), 431–460.

Gehrels, G.E., 2012. Detrital Zircon U-Pb geochronology: Current methods and new opportunities. *In*: Busby, C. and Azor, A. (eds.), *Tectonics of Sedimentary Basins*. Hoboken, New Jersey: Blackwell, pp. 45–62.

Grams, P.E.; Schmidt, J.C., and Topping, D.J., 2007. The rate and pattern of bed incision and bank adjustment on the Colorado River in Glen Canyon downstream of Glen Canyon dam, 1956–2000. *Geological Society of America Bulletin*, 119(5–6) 556–575.

Gray, G.G. and Lawton, T.F., 2011. New constraints on timing of Hidalgoan (Laramide) deformation in the Parras and La Popa basins, NE Mexico. Timing of Hidalgoan deformation in the Parras and La Popa basins. *Boletín de la Sociedad Geológica Mexicana*, 63(2), 333–343.

Heise, E.A.; Benavides, J.A.; Contreras, M.; Cardenas, A., and Lemen, J., 2009. Hurricanes Dolly and Ike damaged the town of South Padre Island from two different directions in 2008. *Shore and Beach*, 77(2), 30–36.

Hernandez-Hinojosa, V.; Montiel-Garcia, P.C.; Armstrong-Altrin, J.S.; Nagarajan, R., and Kasper-Zubillaga, J.J., 2018. Textural and geochemical characteristics of beach sands along the western gulf of Mexico, Mexico. *Carpathian Journal of Earth and Environmental Sciences*, 13(1), 161–174.

Hiatt, T.C., 2010. Sediment Flux Through the Rio Grande River: A Monsoonal Effect. Provo, Utah: Brigham Young University, Master's thesis, 54p.

Jepsen, R.; Chapin, D.M., Jr.; Buhalts, R.; Roberts, J.; Langford, R., and Neu, R., 2003. *Sediment Erosion and Transport at the Rio Grande Mouth, Report for the National Border Technology Program and International Boundary and Water Commission*. Albuquerque, New Mexico: Sandia National Laboratories, 35p.

Kimbrough, D.L.; Grove, M.; Gehrels, G.E.; Dorsey, R.J.; Howard, K.A.; Lovera, O.; Aslan, A.; House, P.K., and Pearthree, P.A., 2015. Detrital zircon U-Pb provenance of the Colorado River: A 5 m.y. record of incision into cover strata overlying the Colorado Plateau and adjacent regions. *Geosphere*, 11(6), 1–30.

Komar, P.D., 1973. Computer models of Delta growth due to sediment input from rivers and longshore transport. *Geological Society of America Bulletin*, 84(7), 2217–2226.

Kondolf, G.M., 1997. Hungry water: Effects of dams and gravel mining on river channels. *Environmental Management*, 21, 533–551.

Larkin, T.J. and Bomar, G.W., 1983. *Climatic Atlas of Texas*. Austin, Texas: Texas Department of Water Resources, *LP-192*, 151p.

Lohse, E.A., 1955. Dynamic geology of the modern coastal region, northwestern Gulf of Mexico. *In*: Hough, J.L. and Menard, H.W. (eds.), *Finding Ancient Shorelines*. *Society of Economic Mineralogists and Paleontologists,* Special Publication No. 3, pp. 99–105.

Mackey, G.N.; Horton, B.K., and Milliken, K.L., 2012. Provenance of the Paleocene-Eocene Wilcox group, western Gulf of Mexico basin: Evidence for integrated drainage of the southern Laramide Rocky Mountains and Cordilleran arc. *Geological Society of America Bulletin*, 124(5–6), 1007–1024.

Malkowski, M.A.; Sharman, G.R.; Johnstone, S.; Grove, M.; Kimbrough, D.L., and Graham, S.A., 2020. Dilution and propagation of provenance trends in sand and mud: Geochemistry and detrital zircon geochronology of modern sediment from central California (USA). *American Journal of Science*, 319(10), 846–902.

Martin, P., 2000. *A Description of the Navy Coastal Ocean Model Version 1.0*. Stennis Space Center, Mississippi: Naval Research Laboratory, 45p.

Masselink, G. and Hughes, M.G., 2003. Fluvial-dominated coastal environments—Deltas. *In*: Davidson-Arnott, R.; Bauer, B., and Houser, C. (eds.), *Introduction to Coastal Processes & Geomorphology*. London: Hodder Arnold, pp. 141–164.

Milliken, K.T.; Anderson, J.B., and Rodriguez, A.B., 2008. A new composite Holocene sea-level curve for the northern Gulf of Mexico. *In:* Anderson, J.B. and Rodriguez, A.B. (eds.), *Response of Upper Gulf Coast Estuaries to Holocene Climate Change and Sea-Level Rise*. Geological Society of America, Special Paper No. 443, pp. 1–11.

Morton, R.A. and Pieper, M.J., 1975. Shoreline changes on Brazos Island and South Padre Island (Mansfield Channel to Mouth of the Rio Grande), an analysis of historical changes of the Texas Gulf Shoreline. Austin, Texas: Bureau of Economic Geology, *Geological Circular 75–2*, 39p.

Morton, R.A., 1994. Texas barriers. *In*: Davis, R.A. (ed.), *Geology of Holocene Barrier Islands*. Berlin, Germany: Springer-Verlag, pp. 75–114.

Moya, J.; Risko, A.; Calvez, K.; Gerkus, H.; Weber, C.; Buckley, K., and Nickerson, B., 2016. *Texas Sediment Sources-General Evaluation Study*. Austin, Texas: Texas General Land Office, 247p.

Nienhuis, J.H.; Ashton, A.D., and Giosan, L., 2015. What makes a delta wave-dominated? *Geology*, 43(6), 511–514.

Nienhuis, J.H.; Ashton, A.D.; Edmonds, D.A.; Hoitink, A.J.F.; Kettner, A.J.; Rowland, J.C., and Törnqvist, T.E., 2020. Global-scale human impact on delta morphology has led to net land area gain. *Nature*, 577, 514–518.

Page, W.R.; VanSistine, D.P., and Turner, K.J., 2005. *Preliminary Geologic Map of Southernmost Texas, United States, and Parts of Tamaulipas and Nuevo Leon, Mexico: Environmental Health Investigations in the United States-Mexico Border Region*. Denver, Colorado: United States Geological Survey, *Open-file report 2005–1409*, 11p., scale 1:250,000.

Press, W.H.; Teukolsky, S.A.; Vetterling, W.T., and Flannery, B.P., 1992. *Numerical Recipes in C: The Art of Scientific Computing*, 2nd edition. New York: Cambridge University Press, 1018p.

Ramos-Vázquez, M.A. and Armstrong-Altrin, J.S., 2019. Sediment chemistry and detrital zircon record from the Bosque and Paseo del Mar coastal areas in the southwestern Gulf of Mexico. *Marine and Petroleum Geology*, 110, 650–675.

Repasch, M.; Karlstrom, K.; Heizler, M., and Pecha, M., 2017. Birth and evolution of the Rio Grande fluvial system in the past 8 Ma: Progressive downward integration and the influence of tectonics, volcanism, and climate: *Earth-Science Reviews*, 168, 113–164.

Ribó, M.; Goodwin, I.D.; O'Brien, P., and Mortlock, T., 2020. Shelf sand supply determined by glacial-age sea-level modes, submerged coastlines and wave climate. *Scientific Reports*, 10, 462.

Rodriguez, A.B.; Fassell, M.L., and Anderson, J.B., 2001. Variations in shoreface progradation and ravinement along the Texas coast, Gulf of Mexico. *Sedimentology*, 48(4), 837–853.

Schoene, B., 2014. U–Th–Pb Geochronology. *In*: Holland, H.D. and Turekian, K.K. (eds.), *Treatise on Geochemistry,* 2nd edition. Oxford: Elsevier, pp. 341–378.

Self, R.P., 1977, Longshore variation in beach sands, Nautla area, Veracruz, Mexico. *Journal of Sedimentary Petrology*, 47(4), 1437–1443.

Seybold, H.; Andrade, J.S., Jr., and Herrmann, H.J., 2007. Modeling river delta formation. *Proceedings of the National Academy of Sciences*, 104(43), 16804–16809.

Sharman, G.R.; Covault, J.A.; Stockli, D.F.; Wroblewski, A.F.J., and Bush, M.A., 2016. Early Cenozoic drainage reorganization of the United States Western Interior–Gulf of Mexico sediment routing system. *Geology*, 45(2), 187–190.

Shideler, G.L., 1978. A sediment dispersal model for the south Texas continental shelf, northwest Gulf of Mexico. *Marine Geology*, 26, 289–313.

Small, E.E.; Blom, T.; Hancock, G.S.; Hynek, B.M., and Wobus, C.W., 2015. Variability of rock erodibility in bedrock-floored stream channels based on abrasion mill experiments. *Journal of Geophysical Research Earth Surfaces*, 120(8), 1455–1469.

Smith, V.B. and Mohrig, D.C., 2017. Geomorphic signature of a dammed Sandy River: The lower Trinity River downstream of Livingston Dam in Texas, USA. *Geomorphology*, 297, 122–136.

Stapor, F.W., 1971. Origin of the Cabo Rojo beach-ridge plain, Veracruz, Mexico. *Gulf Coast Association of Geological Societies Transactions*, 21, 223–230.

Syvitski, J.; Kettner, A.; Overeem, I.; Hutton, E.W.H.; Hannon, M.T.; Brakenridge, G.R.; Day, J.; Vörösmarty, C.; Saito, Y.; Giosan, L., and Nicholls, R.J., 2009. Sinking deltas due to human activities. *Nature Geosciences*, 2, 681–686.

Tapia-Fernandez, H.J.; Armstrong-Altrin, J.S., and Selvaraj, K., 2017, Geochemistry and U–Pb geochronology of detrital zircons in the Brujas beach sands, Campeche, Southwestern Gulf of Mexico, Mexico. *Journal of South American Earth Sciences*, 76, 346–361.

USACE, 1994. *Shore Protection Manual*. Vicksburg, Mississippi: Coastal Engineering Research Center, 316p.

Vidal, V.M.V.; Vidal, F.V., and Perez-Molero, J.M., 1994. Collision of a loop current anticyclonic ring against the continental shelf slope of the western Gulf of Mexico. *Journal of Geophysical Research*, 97(C2), 2155–2172.

Weight, R.W.R.; Anderson, J.B., and Fernandez, R., 2011. Rapid mud accumulation on the central Texas shelf linked to climate change and sea-level rise. *Journal of Sedimentary Research*, 81, 743–764.

Woodroffe, C., 2002, Deltas and estuaries. *In: Coasts: Form, Process and Evolution*. New York: Cambridge University Press, pp. 321–377.

Xu, J.; Stockli, D., and Snedden, J., 2017. Enhanced provenance interpretation using combined U–Pb and (U–Th)/He double dating of detrital zircon grains from lower Miocene strata, proximal Gulf of Mexico basin, North America. *Earth and Planetary Science Letters*. 475, 44–57.

Zavala-Hidalgo, J.; Morey, S.L., and O'Brien, J.J., 2003. Seasonal circulation on the western shelf of the Gulf of Mexico using a high-resolution numerical model. *Journal of Geophysical Research*, 108(C12). doi:10.1029/2003JC001879